


Nonlinear interaction effects in a three-mode cavity optomechanical systemJing Qiu ¹, Li-Jing Jin,^{2,1} Zhen-Yang Peng,^{3,4} Stefano Chesi,^{1,5,*} and Ying-Dan Wang^{3,4,6,†}¹*Beijing Computational Science Research Center, Beijing 100193, China*²*Institute for Quantum Computing, Baidu Research, Beijing 100193, China*³*CAS Key Laboratory of Theoretical Physics, Institute of Theoretical Physics, Chinese Academy of Sciences, P.O. Box 2735, Beijing 100190, China*⁴*School of Physical Sciences, University of Chinese Academy of Sciences, No. 19A Yuquan Road, Beijing 100049, China*⁵*Department of Physics, Beijing Normal University, Beijing 100875, China*⁶*Synergetic Innovation Center for Quantum Effects and Applications, Hunan Normal University, Changsha 410081, China*

(Received 5 January 2022; accepted 2 March 2022; published 18 March 2022)

We investigate the resonant enhancement of nonlinear interactions in a three-mode cavity optomechanical system with two mechanical oscillators. Using the Keldysh Green's function technique, we find that nonlinear effects on the cavity density of states can be greatly enhanced by the resonant interaction of two phononic polaritons, due to their small effective dissipation. In the large detuning limit and taking into account an upper bound on the achievable dressed coupling, the optimal point for probing the nonlinear effect is obtained, showing that such a three-mode system can exhibit significant nonlinear features also for relatively small values of g/κ .

DOI: [10.1103/PhysRevA.105.033514](https://doi.org/10.1103/PhysRevA.105.033514)**I. INTRODUCTION**

Optomechanical systems [1] have witnessed remarkable progress in controlling the quantum state of coupled photonic and mechanical modes. Notable highlights are the demonstration of mechanical ground-state cooling [2–4], generation of strongly squeezed light [5,6] and squeezed mechanical states [7,8], coherent transduction [9], and entanglement of remote mechanical oscillators [10,11]. All these applications are based on a linearized interaction which is dominant under strong optical drive. Continuous technical progress has allowed the dressed coupling G to enter and even surpass the strong-coupling regime [12–15].

On the other hand, nonlinear interactions are necessary for the generation of nonclassical states and a variety of interesting effects have been predicted [16–25]. For these nonlinear signatures the relevant energy scale is the single-photon optomechanical coupling g which unfortunately remains much smaller than both the mechanical frequency ω_m and cavity damping κ in most setups with solid-state mechanical oscillators. Several proposals for effectively enhancing the single-photon coupling strength consider modifying the type of drive, e.g., by introducing a squeezed optical input or a mechanical parametric drive [24,26,27]. Other schemes rely on multimode setups: Systems with two cavity modes [28,29] or multimembrane arrays [30–33] are promising to investigate strong quantum nonlinearities. Recently, it was also proposed that a large enhancement of nonlinear effects could be achieved in optomechanical chains [25]. An attractive feature of the latter scheme is that it is essentially equivalent to

existing setups, developed for efficient nonreciprocity [34,35]. On the other hand, we will show here that the basic mechanism at work in Ref. [25] can be realized by a minimal three-mode setup.

In an optomechanical system, nonlinear effects on the optical density of states (DOS) can be strongly enhanced by a resonance between two polaritons (i.e., the coupled eigenmodes of the linearized system) [21–23]. A main advantage of involving multiple mechanical modes is that two polaritons (instead of one) can be phononic, i.e., have weak hybridization to the optical cavities. In this scenario, the optomechanical nonlinearity results in an indirect phonon-phonon interaction, mediated by the optical modes. Although the effective nonlinear coupling is necessarily smaller than g , the reduction can be more than compensated by the improved coherence of both polaritons, whose lifetime is only limited by the small mechanical damping $\gamma \ll \kappa$. As a result, the optical signatures of nonlinearity can be larger than in a two-mode optomechanical cavity [25].

The above discussion suggests that a single cavity interacting with two mechanical oscillators (see Fig. 1) is the most basic setup where this physics takes place. Indeed, we find that in such a three-mode system the typical figure of merit $(g/\kappa)^2$ of nonlinear effects can be enhanced by a large factor which quite naturally depends on the ratio κ/γ . The enhancement can be optimized with respect to the two mechanical frequencies and doing so we find that it is proportional to $(G/\omega_m)^2$. This conclusion is interesting in view of the recent success in achieving the ultrastrong-coupling regime [15].

The outline of our paper is as follows. In Sec. II we introduce the system and its description in terms of polaritons. Nonlinear effects are studied numerically in Sec. III, while a physical understanding of the results, together with an approximate analytical treatment in terms of phononlike modes,

*stefano.chesi@csrc.ac.cn

†yingdan.wang@itp.ac.cn

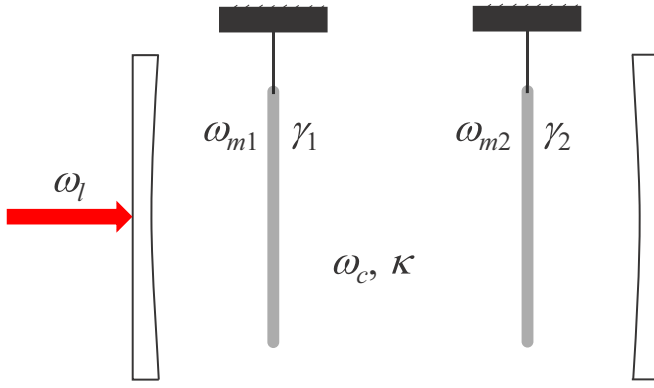


FIG. 1. Schematic illustration of the three-mode optomechanical systems. Here ω_c is the cavity frequency and κ is the cavity damping rate; ω_{mi} are the mechanical frequencies and γ_i are the mechanical damping rates; ω_l is the frequency of the laser drive, represented by the red arrow.

is provided in Sec. IV. We summarize in Sec. V and give some technical details in Appendices A–E.

II. MODEL

As shown in Fig. 1, we consider a driven optomechanical cavity with two mechanical oscillators. The system can be described by the Hamiltonian [1,36,37]

$$H = \omega_c a^\dagger a + \sum_{i=1,2} [\omega_{mi} b_i^\dagger b_i + g_i a^\dagger (b_i + b_i^\dagger)] + (\alpha e^{-i\omega_l t} a^\dagger + \text{H.c.}) + H_{\text{diss}}, \quad (1)$$

where a is the annihilation operator for cavity mode, ω_c is the cavity frequency, b_i ($i = 1, 2$) are the annihilation operators of the mechanical modes, ω_{mi} are the mechanical frequencies (we take $\omega_{m2} \geq \omega_{m1}$), g_i is the single-photon optomechanical coupling, and α is proportional to the amplitude of a classical drive at frequency ω_l . The dissipative Hamiltonian H_{diss} describes independent Markovian baths, with optical and mechanical damping rates κ and $\gamma_{1,2}$, respectively, and is given in Appendix A. The Markovian approximation is usually adequate for optomechanical systems [1,36], except in special circumstances (e.g., relatively strong coupling to nonequilibrium [38] or non-Ohmic [39] reservoirs).

After transforming the cavity mode to a frame rotating at the laser frequency ω_l and performing a displacement transformation $a = \bar{a} + d$ (where \bar{a} is the classical cavity amplitude induced by the laser drive), the Hamiltonian of the system takes the form

$$H_0 = -\Delta d^\dagger d + \sum_{i=1,2} [\omega_{mi} b_i^\dagger b_i + G_i (d + d^\dagger) (b_i + b_i^\dagger)] + g_1 d^\dagger d (b_1 + b_1^\dagger) + g_2 d^\dagger d (b_2 + b_2^\dagger), \quad (2)$$

where $\Delta = \omega_l - \omega_c$ is the detuning and $G_{1,2} = g_{1,2} \bar{a}$ are the dressed couplings which, for definiteness, we take as real. The average number of photons in the cavity is $N = \bar{a}^2$. Throughout this work we focus on a red-detuned laser (i.e., $\Delta < 0$), which allows us to avoid optomechanical instabilities in a

large range of parameters. By neglecting the effect of small damping coefficients κ and $\gamma_{1,2}$, the linearized problem yields the stability condition

$$4G_1^2 \omega_{m2} + 4G_2^2 \omega_{m1} \leq |\Delta| \omega_{m1} \omega_{m2}. \quad (3)$$

A. Polariton eigenmodes

Due to the smallness of the nonlinear interaction, we first diagonalize the linear part of the Hamiltonian. The first line of Eq. (2) can be expressed as

$$H_l = \sum_{i=1}^3 \frac{p_i^2}{2} + \frac{1}{2} \sum_{i,j} x_i M_{i,j} x_j, \quad (4)$$

where x_i and p_i are defined by $b_i = (\omega_{mi} x_i + i p_i) / \sqrt{2\omega_{mi}}$ for $i = 1, 2$ and $d = (|\Delta| x_3 + i p_3) / \sqrt{2|\Delta|}$ for $i = 3$. The dynamical matrix is given by

$$M = \begin{pmatrix} \omega_{m1}^2 & 0 & 2G_1 \sqrt{|\Delta| \omega_{m1}} \\ 0 & \omega_{m2}^2 & 2G_2 \sqrt{|\Delta| \omega_{m2}} \\ 2G_1 \sqrt{|\Delta| \omega_{m1}} & 2G_2 \sqrt{|\Delta| \omega_{m2}} & \Delta^2 \end{pmatrix} \quad (5)$$

and is diagonalized through an (orthogonal) matrix U . Explicitly, $(U^T M U)_{i,j} = \omega_i^2 \delta_{i,j}$, where we conventionally order the eigenmode frequencies as

$$\omega_3 \geq \omega_2 \geq \omega_1. \quad (6)$$

The corresponding Bogoliubov transformation reads

$$(b_1 \ b_2 \ d)^T = V (c_1 \ c_2 \ c_3 \ c_1^\dagger \ c_2^\dagger \ c_3^\dagger)^T \equiv V C^T, \quad (7)$$

where T indicates the transpose and c_i are polariton modes, given by linear combinations of cavity and mechanical modes. We can express the Bogoliubov transformation in terms of U by writing $V = (V_+ \ V_-)$ in block-matrix form, with

$$V_\pm = \begin{pmatrix} U_{11} f_\pm(\frac{\omega_{m1}}{\omega_1}) & U_{12} f_\pm(\frac{\omega_{m1}}{\omega_2}) & U_{13} f_\pm(\frac{\omega_{m1}}{\omega_3}) \\ U_{21} f_\pm(\frac{\omega_{m2}}{\omega_1}) & U_{22} f_\pm(\frac{\omega_{m2}}{\omega_2}) & U_{23} f_\pm(\frac{\omega_{m2}}{\omega_3}) \\ U_{31} f_\pm(\frac{|\Delta|}{\omega_1}) & U_{32} f_\pm(\frac{|\Delta|}{\omega_2}) & U_{33} f_\pm(\frac{|\Delta|}{\omega_3}) \end{pmatrix}, \quad (8)$$

where $f_\pm(x) = (\sqrt{x} \pm \sqrt{1/x})/2$. Clearly, all matrix elements of V are real.

Unfortunately, analytic expressions of U and V are not available in general. The limit of degenerate mechanical frequencies ($\omega_{m1} = \omega_{m2}$) is particularly simple but, as discussed in Appendix B, does not offer any advantage over a basic optomechanical cavity. Instead, it will be interesting to consider a perturbative diagonalization of the general case $\omega_{m2} > \omega_{m1}$ under the condition of large detuning $|\Delta| \gg \omega_{mi}, G_i$. The explicit treatment is presented in Appendix C, leading to approximate expressions for the linear transformation U .

B. Effective two-mode Hamiltonian

Writing the nonlinear interaction in terms of polariton modes, we obtain, for the Hamiltonian in Eq. (2),

$$H_0 = \sum_{i=1}^3 \omega_i c_i^\dagger c_i + (g_{322} c_2^\dagger c_2^\dagger c_3 + g_{311} c_1^\dagger c_1^\dagger c_3 + g_{321} c_2^\dagger c_1^\dagger c_3 + g_{211} c_1^\dagger c_1^\dagger c_2 + \text{H.c.}) + \dots, \quad (9)$$

where we only show explicitly terms of type $c_i^\dagger c_j^\dagger c_k$, having an appreciable effect when the resonance condition $\omega_k = \omega_i + \omega_j$ is satisfied. All remaining terms (of type $c_i^\dagger c_j^\dagger c_k^\dagger$ or $c_i^\dagger c_j^\dagger c_j$) cannot conserve the energy of the unperturbed linear Hamiltonian, and their effect is suppressed by a small factor of order approximately g_{ijk}^2/ω_k (we will work with $\omega_{1,2} \sim \omega_{mi}$ and $\omega_3 \simeq |\Delta| \gg \omega_{mi}$). The system can be tuned to one of the resonances by controlling external parameters, in particular the dressed couplings $G_{1,2}$ and detuning Δ . In the following, we will focus on the condition $\omega_2 = 2\omega_1$, leading to the simple effective model

$$H_0 \simeq \omega_1 c_1^\dagger c_1 + \omega_2 c_2^\dagger c_2 + g_{211}(c_1^\dagger c_1^\dagger c_2 + c_2^\dagger c_1 c_1), \quad (10)$$

where the explicit expression of g_{211} reads

$$g_{211} = \sum_{i=1,2} g_i [V_{3,1} V_{3,2} + V_{3,4} V_{3,5}] (V_{i,1} + V_{i,4}) + V_{3,1} V_{3,4} (V_{i,2} + V_{i,5}). \quad (11)$$

Formally, the problem has been reduced to a system of two interacting polaritons, as in an optomechanical cavity with a single mechanical element [21–23]. However, the regime we will be interested in is very different from that setup, where the two polaritons either have an almost pure optical or mechanical character or (at sufficiently large dressed coupling) are strongly mixed. Here the presence of an additional mechanical mode allows us to consider both low-energy polaritons with a predominantly mechanical character.

To enter this interesting regime, we consider the limit of large detuning $|\Delta| \gg G_i, \omega_{mi}$, leading to $c_{1,2} \simeq b_{1,2}$. Then Eq. (10) can be understood as an effective nonlinear interaction between mechanical modes, mediated by the presence of the cavity. This physical picture will be made more precise through an adiabatic elimination of the optical mode, performed in Sec. IV A and Appendix E. Although the strength of the effective nonlinear interaction is smaller than the bare optomechanical couplings, the effect of the $g_{211} c_2 c_1^\dagger c_1^\dagger$ nonlinear process is greatly enhanced due to the long lifetime of the polariton modes [25]. Inducing a stronger hybridization with the cavity has the beneficial effect of a larger effective interaction g_{211} , but also degrades the coherence of the mechanical modes through the induced optical damping. As we will discuss at length, the competition between these two effects determines the optimal conditions to observe the nonlinearity. The interaction with the optical mode is also important for the optical detection of these phononlike polaritons, leading to narrow signatures in the cavity density of states $\rho_d(\omega)$.

C. Coupling to the reservoirs

By assuming sufficiently small damping rates, satisfying $\kappa, \gamma_{1,2} \ll \omega_i, |\omega_i - \omega_j|$ ($i \neq j$), the coupling of polaritons to the dissipative baths can be treated in the same way as in Refs. [22,23,25]. The Heisenberg-Langevin equations

$$\dot{c}_i = -i\omega_i c_i - \frac{\kappa_i}{2} c_i - \sqrt{\kappa_i} c_{i,\text{in}} \quad (12)$$

are obtained ($i = 1, 2, 3$), where the polariton damping rates are given by

$$\kappa_i = \kappa (V_{3,i}^2 - V_{3,i+3}^2) + \sum_{j=1,2} \gamma_j (V_{j,i} + V_{j,i+3})^2. \quad (13)$$

Here we can recognize distinct contributions from the cavity and phonon baths. The correlation functions $\langle c_{i,\text{in}}^\dagger(t) c_{i,\text{in}}(t') \rangle = n_i \delta(t - t')$ of the noise operators determine the occupation numbers of the polariton modes

$$n_i = \frac{\kappa}{\kappa_i} V_{3,i+3}^2 + \sum_{j=1,2} \frac{\gamma_j}{\kappa_i} (V_{j,i} + V_{j,i+3})^2 n_B(\omega_i), \quad (14)$$

where $n_B(\omega_i) = 1/(e^{\beta\omega_i} - 1)$ is the Bose-Einstein distribution function, evaluated at the frequency of polariton c_i and the (physical) temperature of the two mechanical baths. In the above expression we assume the optical cavity bath to be effectively at zero temperature.

For the convenience of the reader, detailed derivations of these results are presented in Appendices A and D. In particular, in Appendix A we express the system-bath Hamiltonian H_{diss} in terms of polariton modes. A subtle point, which is reflected by the form of Eqs. (13) and (14), concerns the different treatment of the two types of baths. As the mechanical modes are coupled to their bath through $b_j + b_j^\dagger$, an interference between regular ($V_{j,i}$) and anomalous ($V_{j,i+3}$) matrix elements of the Bogoliubov transformation appears. Such an interference is absent for the cavity reservoir because, due to the presence of the laser drive, the rotating-wave approximation has to be performed in a slightly different way [22,23]. We also note that the difference disappears when the anomalous terms are negligible ($V_{j,i+3} \simeq 0$).

In Appendix D we derive the full Heisenberg-Langevin equations leading to Eqs. (13) and (14). There we also include the dissipative coupling between polariton modes and show explicitly that Eq. (12) is justified when $\kappa, \gamma_{1,2} \ll \omega_i, |\omega_i - \omega_j|$. In the following, we will generally assume $\omega_i, |\omega_i - \omega_j| \sim \omega_{mi}$ for the phononlike polaritons, with $\omega_{mi} \gg \kappa \gg \gamma_i$ and $\omega_3 \simeq |\Delta| \gg \omega_{mi}$; thus the conditions leading to Eq. (12) are well satisfied.

III. RESONANT ENHANCEMENT OF NONLINEAR EFFECTS

We now examine the effects of the nonlinear interaction on the cavity DOS $\rho_d(\omega)$,

$$\rho_d(\omega) = -\frac{1}{\pi} \text{Im} G^R[d, d^\dagger; \omega], \quad (15)$$

where $G^R[d, d^\dagger; \omega] = -i \int_0^\infty dt e^{i\omega t} \langle [d(t), d^\dagger(0)] \rangle$ is the retarded Green's function. As shown in Fig. 2, the DOS is characterized by peaks occurring at the polariton frequencies ω_i . Without nonlinear interaction, the peaks have a Lorentzian line shape which, under a suitable resonant condition, gets progressively modified by larger values of $g_{1,2}$. As we focus here on the $\omega_2 = 2\omega_1$ resonance, the largest changes in DOS occur at the $\omega_{1,2}$ peaks. Instead, the third polariton is not involved in the resonant process and the ω_3 peak remains basically unaffected.

Various observable quantities can be related to $\rho_d(\omega)$ and $G^R[d, d^\dagger; \omega]$. In particular, in optomechanically induced

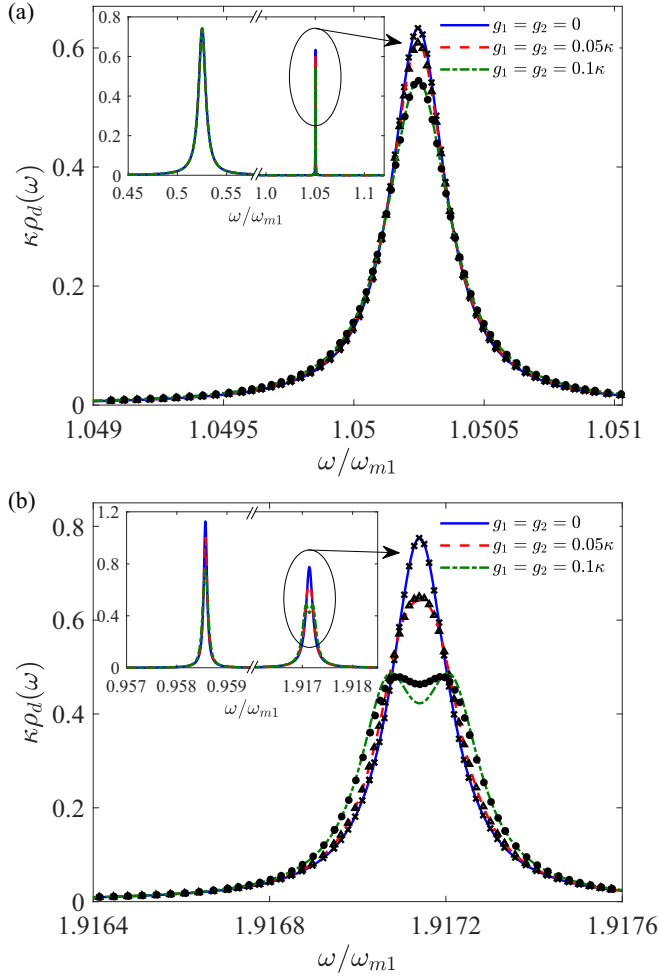


FIG. 2. Cavity DOS in the linear (blue solid curve) and nonlinear regimes (red dashed and green dot-dashed curves) for (a) $\omega_{m2}/\omega_{m1} = 1.1$ and (b) $\omega_{m2}/\omega_{m1} = 1.96$, with $\kappa = 0.02\omega_{m1}$, $\gamma_{1,2} = 10^{-4}\kappa$, $T = 0$, and $G_1 = G_2 = 0.3\omega_{m1}$, leading to resonant detunings (a) $|\Delta| = 1.159\omega_{m1}$ and (b) $|\Delta| = 4.867\omega_{m1}$. These curves are calculated by Eqs. (16), (18), and the perturbative self-energies (19) and (20). The black symbols represent numerical results from a quantum master equation for the $\omega_{1,2}$ polaritons, evaluated with QUTIP [40]. The insets show the DOS in a larger range of ω .

transparency (OMIT) [41,42], the reflection coefficient of a weak probe with frequency ω_p is given by $r(\omega_p) = 1 - i\kappa_{cp}G^R[d, d^\dagger; \omega_p]$ [22,25], where κ_{cp} parametrizes the coupling of the probe field to the input cavity mirror. For sufficiently small κ_{cp} , the reflectivity is directly related to the cavity DOS as $|r(\omega_p)|^2 \simeq 1 - 2\pi\kappa_{cp}\rho_d(\omega_p)$.

To evaluate $\rho_d(\omega)$, it is useful to express Eq. (15) in terms of polariton modes

$$\rho_d(\omega) = -\frac{1}{\pi} \sum_{i,j=1}^6 V_{3,i}V_{3,j} \text{Im}G^R[C_i, C_j^\dagger; \omega], \quad (16)$$

where $C_i = c_i$ and $C_{i+3} = c_i^\dagger$ (with $i = 1, 2, 3$) [see Eq. (7)]. As discussed in Appendix D, the anomalous and off-diagonal ($i \neq j$) components of the polariton Green's functions are small and we will neglect them. Furthermore, if one is interested in frequencies close to a polariton peak, the other

polaritons only induce a small and unstructured off-resonant background. For example, considering the unperturbed limit, the diagonal Green's functions are given by $G_0^R[c_i, c_i^\dagger; \omega] = 1/(\omega - \omega_i + i\kappa_i/2)$. We immediately see that the contribution of an off-resonant polariton j is suppressed by a small factor approximately equal to $\kappa_i\kappa_j/(\omega_i - \omega_j)^2$. A similar suppression occurs for off-diagonal and anomalous contributions [see Eqs. (D9) and (D10)]. These considerations allow us to identify the dominant contributions to the DOS:

$$\rho_d(\omega) \simeq -\frac{V_{3,i}^2}{\pi} \text{Im}G^R[c_i, c_i^\dagger; \omega] \quad \text{for } \omega \simeq \omega_i. \quad (17)$$

The nonlinear interactions can be included by following the treatment developed in Ref. [22] for the two-mode system and extended to multimode optomechanical chains in Ref. [25]. Within this approach, the retarded Green's functions are computed with the Keldysh diagrammatic technique by including the nonlinear interaction H_{nl} through a dominant second-order correction to the self-energy. This approach is justified by the smallness of the nonlinear interaction. Close to the resonant condition $\omega_2 = 2\omega_1$ the nonlinear problem is effectively simplified to a two-mode system and we have

$$G^R[c_i, c_i^\dagger; \omega] = \frac{1}{\omega - \omega_i + i\frac{\kappa_i}{2} - \Sigma_i^R(\omega)}, \quad (18)$$

with the retarded polariton self-energies

$$\Sigma_1^R(\omega) = 4g_{211}^2 \frac{n_1 - n_2}{\omega + \omega_1 - \omega_2 + i(\kappa_1 + \kappa_2)/2}, \quad (19)$$

$$\Sigma_2^R(\omega) = 4g_{211}^2 \frac{n_1 + 1/2}{\omega - 2\omega_1 + i\kappa_1}, \quad (20)$$

and $\Sigma_3^R(\omega) \simeq 0$. The other diagonal Green's functions can be obtained from $G^R[c_i^\dagger, c_i; \omega] = (G^R[c_i, c_i^\dagger; -\omega])^*$ and, as discussed, we neglect off-diagonal and anomalous contributions to Eq. (16).

For representative sets of parameters, the results from this perturbation theory are plotted in Fig. 2. We also show direct numerical simulations of $\rho_d(\omega)$ based on Eq. (10), which take into account g_{211} nonperturbatively. The two approaches are in excellent agreement, except when $g_{211} \sim \kappa_{1,2}$ and the system coupling is beyond the perturbative regime. In practice, it is challenging to realize such large values of the bare couplings $g_{1,2}$ and in the following we will rely on Eqs. (19) and (20).

Finally, we stress the extremely narrow linewidth of the polariton peaks in Fig. 2, which is directly related to the phononlike character of the $\omega_{1,2}$ polaritons. As a consequence, the integrated strength of the optical signal is small. Despite this difficulty, Fig. 2 displays relatively large peak values for $\rho_d(\omega_{1,2})$, of order $1/\kappa$, which is promising for the optical detection of the peaks and their suppression induced by nonlinearity.

A. Resonant curves and approach to instability

To map out the effect of nonlinear interactions as a function of drive strength and detuning, we plot in Fig. 3 the quantity

$$\mathcal{I} = \max_{\omega} |\rho_d(\omega) - \rho_d^0(\omega)|, \quad (21)$$

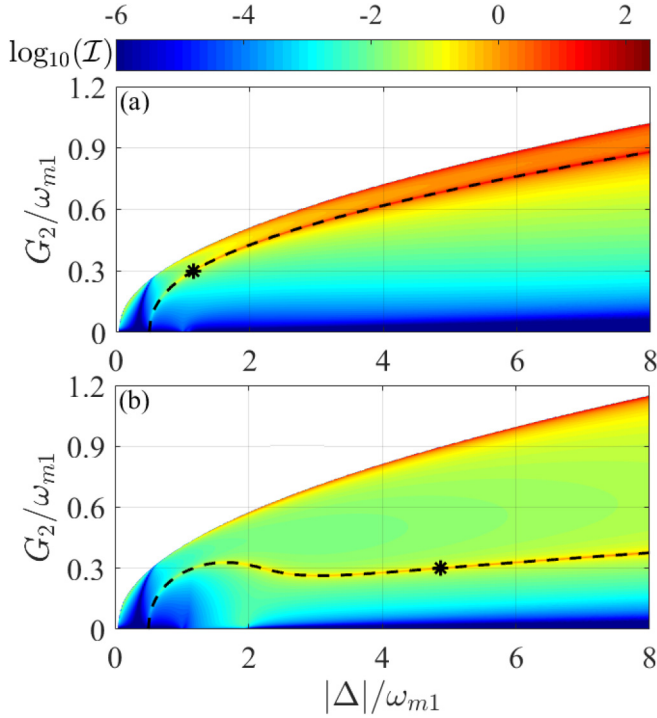


FIG. 3. Dependence of \mathcal{I} on the dressed coupling G_2 and detuning $|\Delta|$, at two fixed values of ω_{m2}/ω_{m1} : (a) 1.1 and (b) 1.96. The boundaries of the colored regions are given by the stability condition (3). The dashed curves show the resonant condition $\omega_2 = 2\omega_1$, obtained from the exact spectrum of Eq. (5). We see that a significant enhancement of nonlinear effects occurs along the resonant curves. In each panel, we have marked explicitly the (Δ, G_2) value corresponding to Fig. 2. The other parameters (taking $\omega_{m1} = 1$) are $\kappa = 0.02$, $\gamma_{1,2} = 2 \times 10^{-6}$, $T = 0$, and $g_1 = g_2 = 2 \times 10^{-4}$ (implying $G_1 = G_2$).

where $\rho_d^0(\omega)$ is the DOS without nonlinearity. As expected, we observe a large enhancement of \mathcal{I} along well-defined curves inside the stability regions, which simply correspond to the condition $\omega_2 = 2\omega_1$. The resonant curves found from the spectrum of Eq. (5) are plotted as dashed lines and match well the enhancement of \mathcal{I} . An increase of \mathcal{I} is also obtained close to the upper boundary of the stable region. Its physical origin is quite different and we will briefly discuss it before returning to the resonant condition for the rest of the article.

When approaching the instability condition, there is a softening of the lowest polariton, $\omega_1 \rightarrow 0$, which is accompanied by anomalous quantum heating, $n_1 \gg 1$. This increase in n_1 leads to a corresponding enhancement of the self-energies (19) and (20). We note, however, that in this regime we are away from resonance and $\Sigma_{1,2}^R(\omega)$ give simple frequency shifts of the polariton lines. For example, in Eq. (20) we can approximate $\Sigma_2^R(\omega) \simeq 4g_{211}^2 n_1 / (\omega_2 - 2\omega_1)$, since $\omega_2 - 2\omega_1 \gg \kappa_{1,2}$. At variance with Fig. 2, the shifts are not accompanied by a significant modification in line shape.

While this behavior should be qualitatively correct, our theory is not accurate in predicting the line shifts. When approaching the instability there is no reason to privilege the $c_1^{\dagger 2} c_2$ term (e.g., the $c_1^{\dagger 3}$ process could give a large contribution). Even before the second-order perturbative treatment

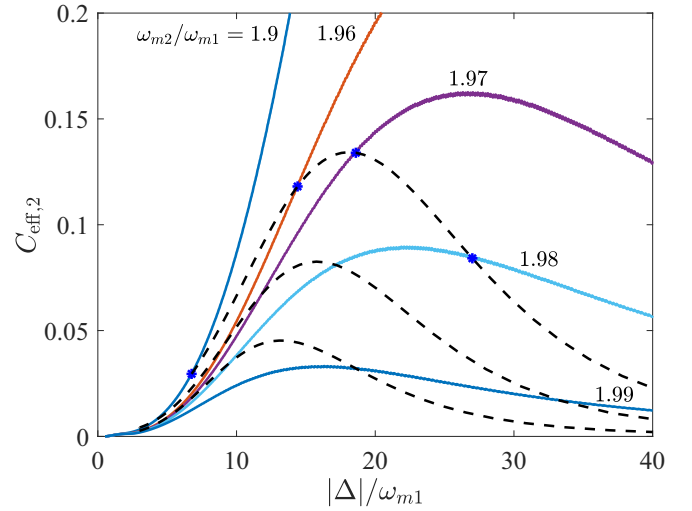


FIG. 4. Dependence of $C_{\text{eff},2}$ on $|\Delta|$ along the resonant curves, at different values of the ratio ω_{m2}/ω_{m1} (as indicated for each solid curve). The dashed lines correspond to the condition $G_{1,2} \leq G_{\text{max}}$, with $G_{\text{max}}/\omega_{m1} = 0.5, 0.4, 0.3$ (top to bottom). For each solid curve, the blue star marks the maximum value of $|\Delta|/\omega_{m1}$ allowed by $G_{1,2} \leq 0.5\omega_{m1}$. The other parameters are the same as in Fig. 3.

breaks down, one should take into account all possible nonlinear terms beyond Eq. (10). In the following we will avoid these difficulties and restrict ourselves to the physically interesting regime around the resonant curves. In particular, we will assume $\omega_2 - 2\omega_1, g_{211} \ll \kappa_{1,2}$, when Eqs. (19) and (20) are justified.

B. Numerical optimization of nonlinear effects

At resonance, we now proceed to discuss the optimal regime to observe the effects of nonlinear interactions. The suppression of $\rho_d(\omega)$ is conveniently characterized through effective cooperativities [22]

$$C_{\text{eff},1} = \frac{16g_{211}^2(n_1 - n_2)}{\kappa_1(\kappa_1 + \kappa_2)}, \quad C_{\text{eff},2} = \frac{4g_{211}^2(1 + 2n_1)}{\kappa_1\kappa_2}, \quad (22)$$

which, by using Eqs. (16)–(20) and the resonant condition $\omega_2 = 2\omega_1$, immediately give

$$\rho_d(\omega_i) \simeq \frac{\rho_d^0(\omega_i)}{1 + C_{\text{eff},i}}. \quad (23)$$

As we will discuss at the end of Sec. IV, the two cooperatives $C_{\text{eff},1}$ and $C_{\text{eff},2}$ are similar at the optimal point (see in particular Fig. 7). Therefore, for definiteness, we will specialize our discussion to $C_{\text{eff},2}$.

Examples of numerically evaluated $C_{\text{eff},2}$ along the resonant lines are shown in Fig. 4 (solid curves). At a given mechanical frequency ratio ω_{m2}/ω_{m1} , the dependence of $C_{\text{eff},2}$ is nonmonotonic. The optimal detuning is determined by a competition between the beneficial decrease in polariton dampings $\kappa_{1,2}$, which eventually saturate to the bare mechanical dissipation rates $\gamma_{1,2}$, and the decrease in the effective nonlinear coupling g_{211} induced by larger values of $|\Delta|$ (a more detailed discussion is provided later on). Another interesting observation is that smaller values of ω_{m2}/ω_{m1} lead to larger values of $C_{\text{eff},2}$. However, this increase in effective

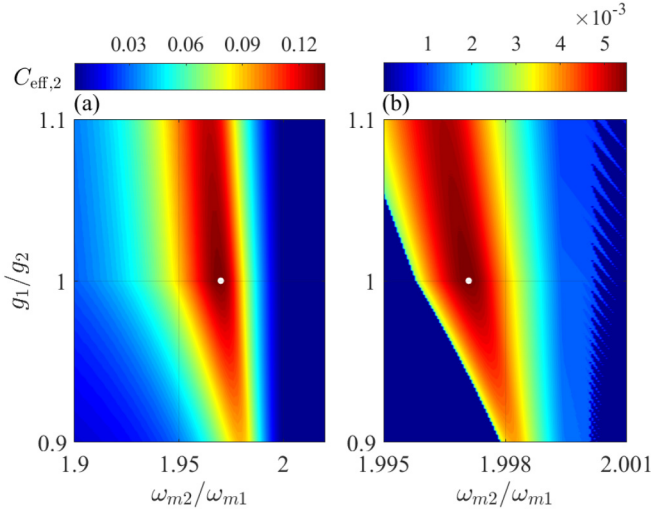


FIG. 5. Maximum value of $C_{\text{eff},2}$ (i.e., optimized over Δ) as a function of ω_{m2}/ω_{m1} and g_1/g_2 , with the restriction $\max[G_1, G_2] \leq G_{\text{max}}$, for (a) $G_{\text{max}} = 0.5\omega_{m1}$ and (b) $G_{\text{max}} = 0.1\omega_{m1}$. The dots mark the optimal values $\tilde{C}_{\text{eff},2}$. We used the following parameters (in units of ω_{m1}): $\kappa = 0.02$, $\max[g_1, g_2] = 2 \times 10^{-4}$, and $\gamma_{1,2} = 2 \times 10^{-6}$.

cooperativity might be impractical, as it is more demanding on the maximum values of dressed couplings $G_{1,2}$.

For example, one can compare the two resonant curves shown in Fig. 3. Clearly, the curve with a smaller value of ω_{m2}/ω_{m1} [Fig. 3(a)] also requires a larger G_2 at any given Δ . A setup achieving $G \simeq 0.4\omega_m$ was only recently demonstrated [15]; thus it is probably more meaningful to perform a comparison assuming equal values of the dressed coupling. This was done in Fig. 2, where $G_{1,2}$ is the same in the two panels. Here the conclusion is reversed: The nonlinear modification of the spectral line is more evident in Fig. 3(b), with a larger value of ω_{m2}/ω_{m1} .

To take these restrictions into account, we consider in Fig. 4 the effect of an upper cutoff $G_{1,2} \leq G_{\text{max}}$. For a few values of G_{max} , the upper bound is shown by the dashed curves. As can be seen, a system with a smaller value of ω_{m2}/ω_{m1} suffers a strong reduction of the maximum allowed value of $|\Delta|$. Therefore, one has to strike a compromise between the generally advantageous effect of reducing ω_{m2}/ω_{m1} and the more restrictive range of $|\Delta|$. The optimal choice of ω_{m2}/ω_{m1} is slightly below 2. For example, we see that the purple curve with $\omega_{m2}/\omega_{m1} = 1.97$ hits the upper dashed boundary close to its maximum and thus represents the optimal choice when $G_{\text{max}} = 0.5\omega_{m1}$.

We also show in Fig. 5 a density plot of the maximum $C_{\text{eff},2}$ (i.e., after optimizing over Δ) as a function of g_1/g_2 and ω_{m2}/ω_{m1} for two different choices of G_{max} . The largest value is marked by a white dot and satisfies $g_1 = g_2$. Instead, the optimal value of ω_{m2}/ω_{m1} is always slightly below 2 but depends on G_{max} .

IV. RESONANCE BETWEEN DRESSED MECHANICAL MODES

In the preceding section we found that the condition $\omega_{m2} \simeq 2\omega_{m1}$ is particularly interesting, as it allows us to maximize the

effect of the nonlinear interaction (see Fig. 5). In this regime the two mechanical modes are already close to the resonant condition, so a small hybridization to the cavity is sufficient to realize $\omega_2 = 2\omega_1$. Furthermore, as illustrated in Fig. 4, the ideal working point is reached by applying a strong drive (giving large values of $G_{1,2}$) at large detuning. This regime of large detuning can be discussed in terms of an effective Hamiltonian for the mechanical modes, obtained after adiabatic elimination of the cavity. This approach is physically more transparent and allows us to obtain approximate expressions for the effective polariton parameters, as well as the maximum of $C_{\text{eff},2}$.

A. Adiabatic elimination

The leading adiabatic contribution to the cavity mode $d(t)$ can be easily derived from the equation of motion

$$d \simeq -\frac{G_1(b_1 + b_1^\dagger) + G_2(b_2 + b_2^\dagger)}{|\Delta|} + \dots, \quad (24)$$

where we have omitted corrections induced by the small dampings and nonlinear interaction, as well as fast-oscillating contributions. A more refined expression, which will become necessary later on, is derived in Appendix E. Eliminating d from Eq. (2) leads to the effective Hamiltonian

$$H_0 \simeq \sum_{i=1,2} \omega_{mi} b_i^\dagger b_i - \frac{[G_1(b_1 + b_1^\dagger) + G_2(b_2 + b_2^\dagger)]^2}{|\Delta|} + \frac{g_1}{G_1 \Delta^2} [G_1(b_1 + b_1^\dagger) + G_2(b_2 + b_2^\dagger)]^3. \quad (25)$$

Furthermore, as we work close to the $\omega_{m2} = 2\omega_{m1}$ condition, the above expression simplifies to

$$H_0 \simeq \sum_{i=1,2} \bar{\omega}_{mi} b_i^\dagger b_i + 3g_1 \frac{G_1 G_2}{\Delta^2} (b_2^\dagger b_1^2 + b_2 b_1^{\dagger 2}), \quad (26)$$

where the shifted mechanical frequencies are given by $\bar{\omega}_{mi} \simeq \omega_{mi} - 2G_i^2/|\Delta|$. Imposing $\bar{\omega}_{m2} = 2\bar{\omega}_{m1}$ gives the desired detuning

$$|\Delta| \simeq \frac{2G_1^2 - G_2^2}{\omega_{m1} - \omega_{m2}/2}. \quad (27)$$

We can also directly read off from Eq. (26) the strength of the effective nonlinear interaction

$$g_{211} \simeq 3g_1 \frac{G_1 G_2}{\Delta^2}. \quad (28)$$

Although, strictly speaking, the derivation of g_{211} should take into account also the correction to Eq. (24) linear in $g_{1,2}$, we show in Appendix E that the final result is unchanged. Equations (27) and (28) are also fully consistent with our previous treatment of polariton modes. When $|\Delta| \gg \omega_{m1}$, $\omega_{m2} \gtrsim G_{1,2}$ we can diagonalize Eq. (5) perturbatively and obtain simplified expressions for the transformation matrix V (defining the Bogoliubov transformation). This approach is discussed in Appendix C. Substituting the approximate V in Eqs. (13), (14), and (11), we recover the same expressions derived within the adiabatic approximation.

To treat the coupling of the mechanical modes to the optical bath, it is necessary to go beyond Eq. (24). The detailed

derivation is given in Appendix E, which leads to the effective dampings ($i = 1, 2$)

$$\kappa_i \simeq \frac{4G_i^2 \omega_{mi}}{|\Delta|^3} \kappa + \gamma_i. \quad (29)$$

Clearly, the total decay rate includes an optical contribution due to the small mixing to the optical cavity (the first term), besides the regular mechanical damping. With the same approach and assuming zero-temperature reservoirs, we also obtain the occupation numbers

$$n_i \simeq \left(\frac{\gamma_i \Delta^2}{\kappa G_i^2} + 4 \frac{\omega_{mi}}{|\Delta|} \right)^{-1}. \quad (30)$$

The finite values of n_i are due to the quantum heating associated with the nonequilibrium conditions, i.e., the presence of the optical drive.

B. Optimal point

By making use of the above expressions, we optimize the visibility of nonlinear effects by maximizing $C_{\text{eff},2}$. By substituting Eqs. (28)–(30) into Eq. (22) we obtain

$$C_{\text{eff},2} \simeq \frac{72\kappa g^2 G_2^6 |\Delta|^3 \left(1 + \frac{\gamma_1 \Delta^2}{2\kappa G_2^2} + 2 \frac{\omega_{m1}}{|\Delta|}\right)}{\left(4G_2^2 \omega_{m1} \kappa + \gamma_1 |\Delta|^3\right)^2 \left(8G_2^2 \omega_{m1} \kappa + \gamma_2 |\Delta|^3\right)}, \quad (31)$$

where we used that, as in Fig. 5, the optimal point occurs for $g_1 = g_2 \equiv g$ (implying $G_1 = G_2$) and $\omega_{m2} \simeq 2\omega_{m1}$. Note that $C_{\text{eff},2}$ characterizes the system at resonance; thus G_2 and Δ are related by Eq. (27). For $G_1 = G_2$, this relation simply reads $|\Delta| = G_2^2 / \delta\omega_m$, where $\delta\omega_m = \omega_{m1} - \omega_{m2}/2$. Setting the dressed coupling at the largest achievable value $G_2 = G_{\text{max}}$, we finally get

$$C_{\text{eff},2} \simeq \frac{72\kappa g^2 G_{\text{max}}^6 / \delta\omega_m^3}{\left(4\omega_{m1} \kappa + \frac{\gamma G_{\text{max}}^4}{\delta\omega_m^3}\right)^2 \left(8\omega_{m1} \kappa + \frac{\gamma G_{\text{max}}^4}{\delta\omega_m^3}\right)}. \quad (32)$$

Here, for simplicity, we assume equal mechanical damping $\gamma_{1,2} = \gamma$ (extension to unequal damping is straightforward). We also set $1 + \gamma_1 \Delta^2 / 2\kappa G_1^2 + 2\omega_{m1}/|\Delta| \simeq 1$ in the numerator of Eq. (31).

Equation (32) approximates the maximum $C_{\text{eff},2}$ at given mechanical frequencies. A comparison to the numerical results is shown in Fig. 6(a), where good agreement is found. As noted previously and also apparent in Fig. 6(a), there is an optimal value of the ratio ω_{m2}/ω_{m1} giving the largest nonlinear effect. We obtain such an optimal point from Eq. (32) as

$$\delta\omega_m \simeq c_0 \left(\frac{\gamma}{\kappa}\right)^{1/3} \left(\frac{G_{\text{max}}}{\omega_{m1}}\right)^{4/3} \frac{\omega_{m1}}{2}, \quad (33)$$

where $c_0 = (\sqrt{5} + 1)^{1/3} \simeq 1.5$. Since usually $\gamma \ll \kappa$, Eq. (33) represents a small deviation from $\omega_{m2} = 2\omega_{m1}$. The inset of Fig. 6(a) shows that a larger dressed optomechanical coupling G_{max} causes the optimal ratio ω_{m2}/ω_{m1} to move farther away from $\omega_{m2} = 2\omega_{m1}$, besides allowing for more prominent nonlinear effects, which is in agreement with Eq. (33). Finally, by using the optimal $\delta\omega_m$ we obtain

$$\tilde{C}_{\text{eff},2} \simeq (c_1 R + c_2 R^{2/3} + \dots) \left(\frac{g}{\kappa}\right)^2, \quad (34)$$

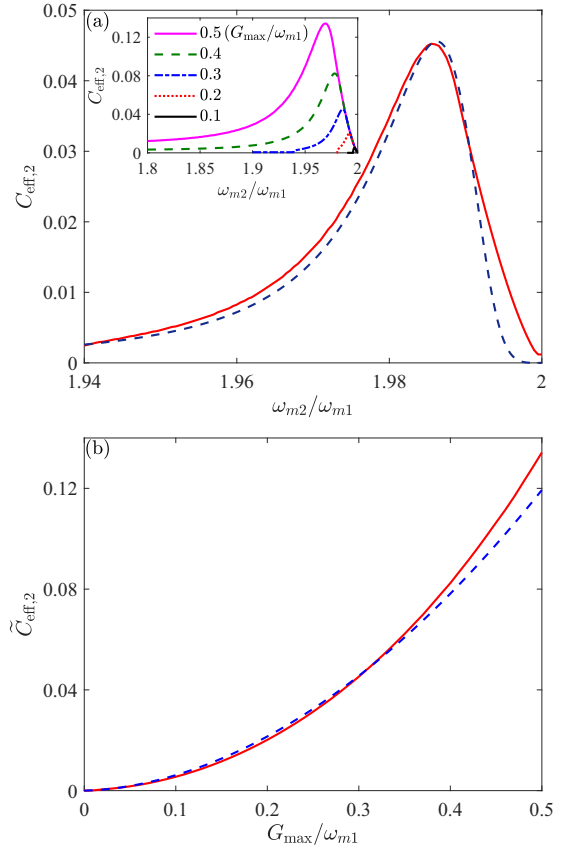


FIG. 6. (a) Dependence of $C_{\text{eff},2}$ on ω_{m2}/ω_{m1} , obtained after optimizing Δ with $g_1/g_2 = 1$ and $G_{1,2} \leq G_{\text{max}}$. The main panel is for $G_{\text{max}}/\omega_{m1} = 0.3$ and presents a comparison of the numerical curve (solid) to the approximate treatment (dashed), described by Eqs. (31) and (27). The curves in the inset are obtained numerically and illustrate the effect of changing $G_{\text{max}}/\omega_{m1}$. In particular, the $G_{\text{max}}/\omega_{m1} = 0.1$ and 0.5 curves are line cuts of Fig. 5. (b) Dependence of the fully optimized cooperativity $\tilde{C}_{\text{eff},2}$ on $G_{\text{max}}/\omega_{m1}$. The dashed curve is the approximate equation (34). In both panels we used (in units of ω_{m1}) $\kappa = 0.02$, $\gamma_{1,2} = 2 \times 10^{-6}$, and $g_{1,2} = 2 \times 10^{-4}$.

where the numerical prefactors are $c_1 = 9(5\sqrt{5} - 11)/4 \approx 0.41$ and $c_2 = 9(7 - 3\sqrt{5})/\sqrt[3]{16(\sqrt{5} - 1)} \approx 0.97$. Here we have defined the important parameter

$$R = \left(\frac{G_{\text{max}}}{\omega_{m1}}\right)^2 \frac{\kappa}{\gamma}, \quad (35)$$

which we assumed large, $R \gg 1$, to obtain an enhancement of $C_{\text{eff},2}$ with respect to the typical figure of merit $(g/\kappa)^2$ [22]. Entering the favorable regime of large R is facilitated by the typically large value of κ/γ . Since in Eq. (34) the prefactor is expressed through powers of R , the fully optimized cooperativity $\tilde{C}_{\text{eff},2}$ exhibits a monotonic dependence on G_{max} . In Fig. 6(b) we show that the increase of $\tilde{C}_{\text{eff},2}$ is well described by the approximate equation (34).

C. Application to electromechanical setups

Motivated by the increase with G_i , we now estimate the achievable values of $\tilde{C}_{\text{eff},2}$, taking as reference the recent electromechanical setup of Ref. [15]. Here, using a three-

TABLE I. Parameters from two specific setups.

Parameter	Ref. [15]	Ref. [13]
$\omega_c/2\pi$	6.506 GHz	7.47 GHz
$\kappa/2\pi$	1.2 MHz	170 kHz
$\omega_m/2\pi$	9.696 MHz	10.69 MHz
$\gamma/2\pi$	31 ± 1 Hz	30 Hz
$g/2\pi$	167 ± 2 Hz	230 Hz
$G_{\max}/2\pi$	3.83 MHz	0.5 MHz

dimensional superconducting cavity, ultrastrong parametric couplings of order $G_{\max} \sim 0.4\omega_m$ are achieved. From Eq. (34) and with the parameters listed in Table I (second column), we obtain $\tilde{C}_{\text{eff},2} \simeq 0.5 \times 10^{-4}$ in the three-mode system. Although this figure of merit is small, a useful reference is the value of \tilde{C}_{eff} for a two-mode setup [21–23]. The optimal point is at $\Delta \simeq -2\omega_m$, leading to

$$C_{\text{eff}} \simeq \frac{45}{8} \frac{g^2}{\kappa^2} \quad (36)$$

(two modes). The physical regime here is different, as one of the two interacting polaritons is a weakly perturbed cavity mode. The nonlinear interaction with the phononlike polariton can be detected as a narrow dip on top of the broad optical peak. For this scenario, one would get $C_{\text{eff}} \simeq 10^{-7}$. The larger value of the three-mode system is due to the enhancement factor, of order $R \simeq 6 \times 10^3$, which allows us to take advantage of the ultrastrong-coupling regime.

It is also instructive to consider parameters from an electromechanical setup with lumped elements (third column of Table I) and a much smaller $G_{\max} \sim 0.05\omega_m$. Here we only have $R \simeq 12$ and we estimate that the three-mode system could achieve $\tilde{C}_{\text{eff},2} \simeq 2 \times 10^{-5}$. This value is only slightly smaller than the first setup (with ultrastrong parametric couplings), as it takes advantage of a larger ratio g/κ . In the first example, the value of $\tilde{C}_{\text{eff},2}$ suffers from the relatively large damping of the microwave cavity κ . Improving that parameter to the approximately 100 kHz range would result in a much larger value of $(g/\kappa)^2$, thus approaching $\tilde{C}_{\text{eff},2} \simeq 10^{-3}$.

Finally, we note that the working point of Ref. [15] is at $\Delta = -\omega_m$, when the dressed optomechanical coupling is limited by the optomechanical instability to $G_{\max} < 0.5\omega_m$. However, here we consider larger values of $|\Delta|$. The onset of the instability would be much less restrictive on the achievable values of G_{\max} , with potential benefits on the enhancement of nonlinear effects.

D. Estimation of relevant scales

Based on the effective parameters of the polariton modes, given in Sec. IV A, we estimate the position of interesting working points and derive in a simpler manner some general parameter dependences. We start by considering the maximum of $C_{\text{eff},2}$ as a function of detuning, illustrated in Fig. 4. This optimal point has a simple physical origin, as it occurs when the induced optical damping [the first term of Eq. (29)] becomes smaller than the mechanical damping γ . At larger detunings the polariton damping rates become approximately constant, i.e., $\kappa_i \sim \gamma$, and $C_{\text{eff},2}$ suffers from the decrease of

interaction strength g_{211} between phononlike polaritons. More precisely, we estimate this condition from Eq. (29) as

$$\frac{G_1^2 \omega_{m1}}{|\Delta|^3} \kappa \sim \gamma, \quad (37)$$

and using that at resonance $|\Delta| \simeq G_1^2/\delta\omega_m$ we obtain the optimal detuning

$$|\Delta^*| \sim \sqrt{\frac{\kappa}{\gamma} \omega_{m1} \delta\omega_m}. \quad (38)$$

Below $|\Delta^*|$, the growth of $C_{\text{eff},2}$ with $|\Delta|$ is due to the improved coherence properties of the $i = 1, 2$ polaritons. In particular, when $|\Delta| \ll |\Delta^*|$ we can neglect the mechanical dampings in the expressions of κ_i . Setting $\gamma_{1,2} = 0$ in Eq. (31) and also neglecting $2\omega_{m1}/|\Delta|$ in the numerator (since $|\Delta| \gg \omega_{m1}$), we indeed obtain a monotonically increasing function

$$C_{\text{eff},2} \simeq \frac{9}{16} \left(\frac{g}{\kappa}\right)^2 \left(\frac{|\Delta|}{\omega_{m1}}\right)^3. \quad (39)$$

The cubic dependence of $C_{\text{eff},2}$ can be traced as follows. The product $\kappa_1\kappa_2$ of damping rates contributes to an enhancement factor approximately equal to $(|\Delta|/\omega_{m1})^4$ to the effective cooperativity (22). The increase of n_1 is approximately $|\Delta|/4\omega_{m1}$ and can also be attributed to the smaller polariton damping [see the small κ_i denominator in Eq. (14)]. On the other hand, as expected, the effective interaction g_{211} is always suppressed by a larger detuning [see Eq. (28)]. The final result is the cubic enhancement factor $(|\Delta|/\omega_{m1})^3$.

A rough estimate of the maximum $C_{\text{eff},2}$ is obtained by evaluating Eq. (39) at $\Delta = \Delta^*$:

$$C_{\text{eff},2} \lesssim \left(\frac{g}{\kappa}\right)^2 \left(\frac{\kappa \delta\omega_m}{\gamma \omega_{m1}}\right)^{3/2}. \quad (40)$$

Since $\delta\omega_m/\omega_{m1} = 1 - \omega_{m2}/2\omega_{m1}$ we see that, in principle, it is advantageous to move away from the condition $\omega_{m2} = 2\omega_{m1}$. However, as discussed, we should take into account practical limitations on the achievable $G_{1,2}$. With $G_{1,2} \leq G_{\max}$, the maximum allowed value of $|\Delta|$ is given by Eq. (27), where the factor $1 - \frac{\omega_{m2}}{2\omega_{m1}}$ appears in the denominator (i.e., the allowed range shrinks by reducing ω_{m2}/ω_{m1}). An approximate criterion to estimate the optimal ω_{m2}/ω_{m1} is to impose that the range of allowed values of Δ extends roughly up to the maximum in $C_{\text{eff},2}$. Equating Eqs. (27) and (38) yields

$$\delta\omega_m \sim \left(\frac{\gamma}{\kappa}\right)^{1/3} \left(\frac{G_{\max}}{\omega_{m1}}\right)^{4/3} \omega_{m1} \quad (41)$$

and substituting this estimate in Eq. (40), we obtain

$$\tilde{C}_{\text{eff},2} \sim \left(\frac{g}{\kappa}\right)^2 \frac{\kappa}{\gamma} \left(\frac{G_{\max}}{\omega_{m1}}\right)^2. \quad (42)$$

Equations (41) and (42) are in agreement with the more precise expressions (33) and (34), respectively. Through this discussion, we see that the optimal values arise from a competition between the reduction in the effective optical damping at large $|\Delta|$ and the presence of a residual mechanical damping, together with practical restrictions in achieving sufficiently large dressed optomechanical couplings.

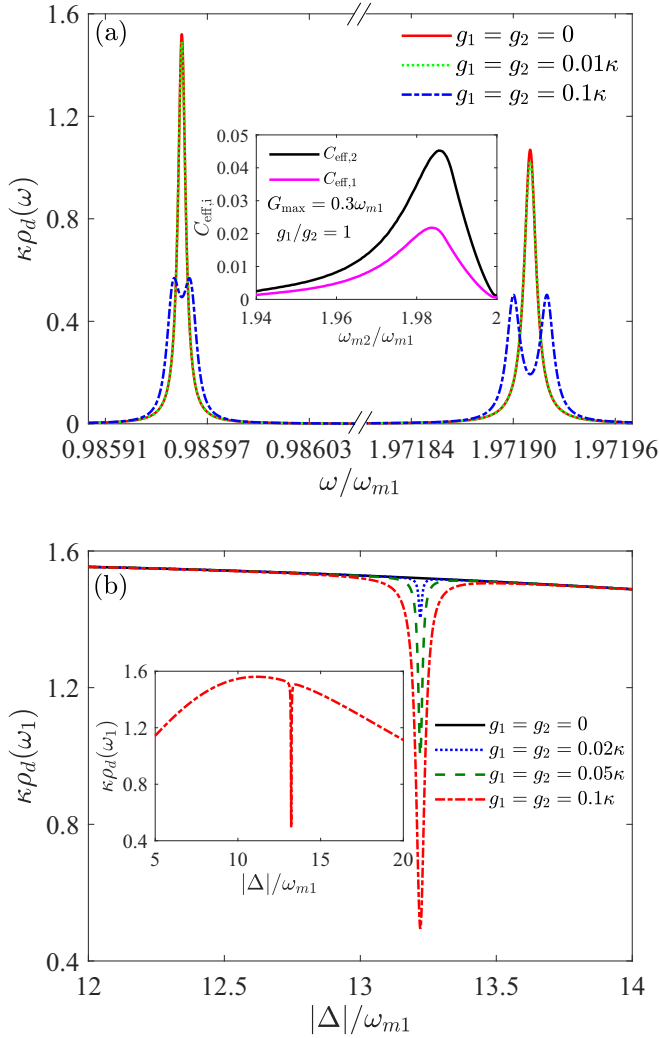


FIG. 7. (a) Comparison of the cavity DOS in the linear (red solid curve) and nonlinear regimes, using $g_{1,2} = 0.01\kappa$ (green dotted curve) and $g_{1,2} = 0.1\kappa$ (blue dot-dashed curve). We also used $|\Delta| = 13.22\omega_{m1}$, $G_2 = 0.3\omega_{m1}$, $\omega_{m2}/\omega_{m1} = 1.9858$, $\kappa = 0.02\omega_{m1}$, and $\gamma_{1,2} = 10^{-4}\kappa$. In the inset we show a comparison of $C_{\text{eff},1}$ (bottom curve) and $C_{\text{eff},2}$ (top curve). The two curves are already optimized over Δ , with $g_{1,2} = 0.01\kappa$. The other parameters are the same as in the main plot. (b) Dependence of $\rho_d(\omega_1)$ as a function of Δ for several values of $g_1 = g_2$. We used $g_1 = 0, 0.02\kappa, 0.05\kappa, 0.1\kappa$ (from top to bottom). The other parameters are the same as in (a). The sharp dip corresponds to the resonant condition and becomes more pronounced at larger values of $g_{1,2}$. The inset shows the $g_1 = 0.1\kappa$ curve in a larger range of Δ .

E. Line shape and lower polariton

We conclude this section by discussing the qualitative change of line shape induced by nonlinear effects. Since here the damping rates of the two polaritons are comparable [see, for example, below Eq. (37), where we have obtained $\kappa_2 \simeq 2\kappa_1$], the spectral line shape is not modified qualitatively at small g . This behavior is illustrated by the $g = 0.01\kappa$ curves of Fig. 7(a) and is distinct from what happens in a two-mode system, where a sharp dip can be induced at the higher polariton peak for very small values of g [21–23].

Therefore, similar to the four-mode optomechanical ring [25], the nonlinear effects could be more easily demonstrated by tuning external parameters like Δ and G_i across the resonant condition $\omega_2 = 2\omega_1$. As shown in Fig. 7(b), changing Δ will induce a sharp feature in the dependence of the density of states (or a related observable, e.g., the OMIT signal [23,25]).

Instead, if the optomechanical coupling can be made larger, we enter a regime where two distinct resonances appear, as illustrated in Fig. 7 by assuming $g_{1,2} = 0.1\kappa$. The splittings of the ω_1 and ω_2 polariton peaks are given by

$$\delta_1 \simeq 4g_{211}\sqrt{n_1 - n_2}, \quad \delta_2 \simeq 4g_{211}\sqrt{n_1 + \frac{1}{2}}, \quad (43)$$

respectively, and they are resolved when $\delta_{1,2} \gtrsim \kappa_{1,2}$.

Figure 7(a) also shows that the nonlinear effects at the upper (ω_2) and lower (ω_1) polaritons are comparable. This fact can be checked from our previous analytical expressions: In the regime of negligible $\gamma_{1,2}$ we have $\kappa_2/\kappa_1 \simeq n_1/n_2 \simeq 2$, leading to $C_{\text{eff},1} \simeq \frac{2}{3}C_{\text{eff},2}$ [based on Eq. (22)]. On the other hand, around the maximum of the effective cooperativity we can estimate $\kappa_2/\kappa_1 \simeq n_1/n_2 \simeq \frac{3}{2}$, leading to $C_{\text{eff},1} \simeq \frac{2}{5}C_{\text{eff},2}$.

V. CONCLUSION

In this paper we have investigated nonlinear interaction effects in a three-mode cavity optomechanical system with one cavity mode and two mechanical modes. To take full advantage of the two mechanical modes, we concentrated on a regime where a resonant interaction of phononlike polaritons takes place. Due to the very small polariton dissipation rates, nonlinear effects on the cavity density of states and related observables could be greatly enhanced. In the large detuning limit and considering an upper bound on the largest achievable dressed coupling, we obtained the optimal value of nonlinear effects. Our analytic expressions indicate that the typical figure of merit is enhanced by a parameter which can be large, being proportional to the ratio κ/γ .

Although with small single-photon optomechanical couplings $g_{1,2}$ the nonlinear effects only induce a slight modification of the spectral line shape, it would still be possible to observe sharp features by tuning system parameters across the resonant condition. On the other hand, if a regime of sufficiently large $g_{1,2}$ can be reached, the splittings of the ω_1 and ω_2 polariton peaks are clearly established. Furthermore, the present setup can realize a mechanical analog of parametric oscillation and second harmonic generation, if either one of the phononlike polaritons is driven by an external laser, and might facilitate the observation of non-classical photon correlations induced by the optomechanical interaction [16,17,24,28].

ACKNOWLEDGMENTS

S.C. acknowledges support from the National Key Research and Development Program of China (Grant No. 2016YFA0301200), NSAF (Grant No. U1930402), NSFC (Grants No. 11974040 and No. 12150610464), and a Cooperative Program by the Italian Ministry of Foreign Affairs and International Cooperation (Program No. PGR00960). Y.-D.W. acknowledges support from NSFC (Grant No. 11947302) and MOST (Grant No. 2017FA0304500). L.-J.J. acknowledges

support from NSFC (Grant No. 11804020). We gratefully acknowledge helpful discussions with A. A. Clerk.

APPENDIX A: POLARITON-BATH INTERACTION

We start from the system-bath Hamiltonian H_{diss} , given in terms of the bare cavity and mechanical modes

$$\begin{aligned} H_{\text{diss}} = & \sum_j \omega_{c,j} f_{c,j}^\dagger f_{c,j} + \sum_{\alpha=1,2} \sum_j \omega_{\alpha,j} f_{\alpha,j}^\dagger f_{\alpha,j} \\ & - i \sum_j \sqrt{\frac{\kappa}{2\pi\rho_c}} (f_{c,j} - f_{c,j}^\dagger)(a + a^\dagger) \\ & - i \sum_{\alpha=1,2} \sum_j \sqrt{\frac{\gamma_\alpha}{2\pi\rho_\alpha}} (f_{\alpha,j} - f_{\alpha,j}^\dagger)(b_\alpha + b_\alpha^\dagger), \quad (\text{A1}) \end{aligned}$$

where $f_{\alpha,j}$ are the annihilation operators for the mechanical ($\alpha = 1, 2$) and cavity ($\alpha = c$) bath modes, with corresponding frequencies $\omega_{\alpha,j}$ ($\alpha = 1, 2, c$). As in the main text, κ is the damping rate of photons inside the cavity and $\gamma_{1,2}$ are the two mechanical damping rates. Furthermore, ρ_c is the cavity-bath density of states and $\rho_{1,2}$ are the mechanical density of states. Because we consider Markovian baths, we take κ , ρ_c , γ_α , and ρ_α to be frequency independent.

We derive the appropriate polariton-bath Hamiltonian analogously to the two-mode system [22,23], by first transforming all optical modes (both cavity and bath modes) to a frame rotating at ω_l and applying suitable displacement transformations. The final form of the Hamiltonian is similar to Eq. (A1), except for the replacements $\omega_{c,j} f_{c,j}^\dagger f_{c,j} \rightarrow \Delta_{c,j} g_{c,j}^\dagger g_{c,j}$, where $\Delta_{c,j} = \omega_{c,j} - \omega_l$ is shifted by the drive frequency. Furthermore, $(f_{c,j} - f_{c,j}^\dagger)(a + a^\dagger) \rightarrow (g_{c,j} d^\dagger - g_{c,j}^\dagger d)$. We have neglected the counterrotating terms in the interaction with the optical bath, as they are proportional to $e^{\pm 2i\omega_l t}$. Finally, we express d and $b_{1,2}$ in terms of polariton operators

$$\begin{aligned} H_{\text{diss}} = & \sum_j \Delta_{c,j} g_{c,j}^\dagger g_{c,j} + \sum_{\alpha=1,2} \sum_j \omega_{\alpha,j} f_{\alpha,j}^\dagger f_{\alpha,j} \\ & - i \sum_{k=1,2,3} \sum_j \sqrt{\frac{\kappa}{2\pi\rho_c}} [g_{c,j} (V_{3,k} c_k^\dagger + V_{3,k+3} c_k) - \text{H.c.}] \\ & - i \sum_{\alpha,k} \sum_j \sqrt{\frac{\gamma_\alpha}{2\pi\rho_\alpha}} [(V_{\alpha,k} + V_{\alpha,k+3}) f_{\alpha,j} c_k^\dagger - \text{H.c.}], \quad (\text{A2}) \end{aligned}$$

where $\alpha = 1, 2$ labels the mechanical modes and $k = 1, 2, 3$ labels the polaritons. In the last line, representing the interaction of polaritons with mechanical reservoirs, we have performed the rotating-wave approximation, since $\omega_{\alpha,j} > 0$ and the counterrotating terms of type $f_{\alpha,j} c_k$ cannot conserve the energy. On the other hand, the counterrotating terms of type $g_{c,j} c_k$ should be retained, since $\Delta_{c,j} > -\omega_l$ (with ω_l much larger than the polariton frequencies).

The different way in which the rotating-wave approximation is performed on the optical and mechanical bath modes is due to the presence of the cavity drive. A more detailed discussion of the treatment can be found in Refs. [22,23,25], while here we only make two remarks. (i) The presence of counterrotating terms in the second line of Eq. (A2) leads

to heating of the polaritons even when the cavity bath is at zero temperature, a phenomenon which can be referred to as quantum heating. Physically, the polaritons can be excited through the absorption of photons from the drive. (ii) Since $f_{\alpha,j}$ is coupled to $b_\alpha + b_\alpha^\dagger$ [see Eq. (A1)] and the Bogoliubov transformation has anomalous terms, i.e., b_α involves both c_k and c_k^\dagger [see Eq. (7)], the coupling coefficient of $f_{\alpha,j} c_k^\dagger$ displays an interference of $f_{\alpha,j} b_\alpha$ and $f_{\alpha,j} b_\alpha^\dagger$ contributions. This does not happen for the optical bath, where the $g_{c,j} d_\alpha$ interaction was neglected from the onset. Again, this difference can be traced to the presence (absence) of driving on the optical (mechanical) modes.

An equivalent way to treat the interaction with the bath is through the Langevin equations. For the mechanical modes, which are coupled to the bath through the X quadrature, the most appropriate form of the dissipation terms is $\dot{b}_\alpha = -\frac{\gamma_\alpha}{2}(b_\alpha + b_\alpha^\dagger) + \dots$. Instead, the Langevin equation of the driven optical mode reads $\dot{d} = -\frac{\kappa}{2}d + \dots$, in agreement with previous discussions on the rotating-wave approximation of H_{diss} (after taking into account the drive). This difference, combined with the anomalous terms of the Bogoliubov transformation, leads to the presence (absence) of interference in κ_i when writing the Langevin equations in terms of polariton modes.

APPENDIX B: EQUAL MECHANICAL FREQUENCIES

When the two mechanical resonators have the same frequency, i.e., $\omega_{m1} = \omega_{m2} = \omega_m$, the system becomes equivalent to a two-mode optomechanical cavity. This is easily seen by introducing the mechanical dark mode b_- [43], together with the bright mode b_+ ,

$$b_- = \frac{G_1 b_2 - G_2 b_1}{\tilde{G}}, \quad (\text{B1})$$

$$b_+ = \frac{G_1 b_1 + G_2 b_2}{\tilde{G}}, \quad (\text{B2})$$

with $\tilde{G} = \sqrt{G_1^2 + G_2^2}$. Hence, we rewrite the Hamiltonian (2) as

$$\begin{aligned} H_0 = & -\Delta d^\dagger d + \omega_m b_+^\dagger b_+ + \omega_m b_-^\dagger b_- \\ & + \tilde{G}(d + d^\dagger)(b_+ + b_+^\dagger) + \tilde{g} d^\dagger d (b_+ + b_+^\dagger), \quad (\text{B3}) \end{aligned}$$

where $\tilde{g} = \tilde{G}/\sqrt{N}$. We see that only the bright mode b_+ interacts with the cavity and the optomechanical interaction has the standard form. That is to say, the three-mode cavity system has been transformed to a standard two-mode optomechanical setup, with an independent mechanical dark mode.

APPENDIX C: APPROXIMATE FORM OF V

In this Appendix we present the approximate form of V in the large detuning limit $|\Delta| \gg \omega_{mi}, G_i$. We first perform a block diagonalization of M using quasidegenerate perturbation theory

$$e^{-S} M e^S \simeq \begin{pmatrix} \omega_{m1}^2 - B_{11}^2 & -B_{12}^2 & 0 \\ -B_{21}^2 & \omega_{m2}^2 - B_{22}^2 & 0 \\ 0 & 0 & \Delta^2 + B_{11}^2 + B_{22}^2 \end{pmatrix}, \quad (\text{C1})$$

where the B_{ij}^2 are second-order corrections with respect to the unperturbed matrix $M_{i,j}^{(0)} = \Delta^2 \delta_{3,i} \delta_{3,j}$:

$$B_{ij}^2 = \frac{4}{|\Delta|} G_i G_j \sqrt{\omega_{mi} \omega_{mj}}. \quad (\text{C2})$$

To lowest order, the transformation matrix S is given by

$$S \simeq \frac{1}{|\Delta|} \begin{pmatrix} 0 & 0 & B_{11} \\ 0 & 0 & B_{22} \\ -B_{11} & -B_{22} & 0 \end{pmatrix}. \quad (\text{C3})$$

The eigenvalues of Eq. (C1) are the normal mode frequencies ω_i and are easily obtained as follows:

$$\omega_{1,2}^2 \simeq \frac{1}{2} (\omega_{m1}^2 + \omega_{m2}^2 - B_{11}^2 - B_{22}^2 \mp \sqrt{(\omega_{m1}^2 - \omega_{m2}^2 - B_{11}^2 + B_{22}^2)^2 + 4B_{12}^4}), \quad (\text{C4})$$

$$\omega_3^2 \simeq \Delta^2 + B_{11}^2 + B_{22}^2. \quad (\text{C5})$$

The sign in Eq. (C4) is chosen to satisfy $\omega_2 \geq \omega_1$.

Diagonalization of Eq. (C1) is through a rotation by an angle given by $\tan 2\theta = 2B_{12}^2/(\omega_{m2}^2 - \omega_{m1}^2 + B_{11}^2 - B_{22}^2)$. Finally, combining e^S and the rotation by θ , we find an approximate expression for U :

$$U \simeq \begin{pmatrix} \cos \theta & -\sin \theta & \frac{B_{11}}{|\Delta|} \\ \sin \theta & \cos \theta & \frac{B_{22}}{|\Delta|} \\ -\frac{B_{11} \cos \theta + B_{22} \sin \theta}{|\Delta|} & \frac{B_{11} \sin \theta - B_{22} \cos \theta}{|\Delta|} & 1 \end{pmatrix}. \quad (\text{C6})$$

Equation (C6) can be inserted in Eq. (8) to get the desired approximate form of V . For example, to evaluate κ_i from Eq. (13) we need the quantities

$$\begin{aligned} V_{3,i}^2 - V_{3,i+3}^2 &= U_{3,i}^2, \\ (V_{j,i} + V_{j,i+3})^2 &= U_{j,i}^2 \frac{\omega_{mj}}{\omega_i}, \end{aligned} \quad (\text{C7})$$

which are readily obtained from Eq. (C6). If $G_i \lesssim \omega_{m1}, \omega_{m2}$, the rotation angle θ is small. Thus, in Eq. (C7) we can approximate $U_{1,1} = U_{2,2} = 1$ and $U_{1,2} = U_{2,1} = 0$, giving $\kappa_{1,2}$ as in Eq. (29). Equations (28) and (30) can be obtained in a similar way.

APPENDIX D: EQUATIONS OF MOTION IN THE LINEAR REGIME

We give here the Heisenberg-Langevin equations of the polariton modes in the linear approximation. The present analysis, by retaining explicitly off-diagonal damping terms, extends previous treatments [22,23,25] and allows us to discuss the off-diagonal Green's functions.

We consider the quadratic Hamiltonian $H_l + H_{\text{diss}}$, where $H_l = \sum_k \omega_k c_k^\dagger c_k$ and H_{diss} is given in Eq. (A2). Then the Heisenberg-Langevin equations can be derived in a standard way and take the form ($i = 1, 2, 3$)

$$\dot{c}_i = -i\omega_i c_i - \sum_{j=1}^3 \left(\frac{\kappa_{ij}}{2} c_j + \frac{\bar{\kappa}_{ij}}{2} c_j^\dagger \right) - \sqrt{\kappa_i} c_{i,\text{in}}, \quad (\text{D1})$$

where

$$\begin{aligned} \kappa_{ij} &= \kappa (V_{3,i} V_{3,j} - V_{3,i+3} V_{3,j+3}) \\ &+ \sum_{k=1,2} \gamma_k (V_{k,i} + V_{k,i+3})(V_{k,j} + V_{k,j+3}), \end{aligned} \quad (\text{D2})$$

$$\bar{\kappa}_{ij} = \kappa (V_{3,i} V_{3,j+3} - V_{3,j} V_{3,i+3}). \quad (\text{D3})$$

The matrix κ_{ij} is symmetric and the diagonal elements $\kappa_{ii} \equiv \kappa_i$ are in agreement with Eq. (13). Instead, $\bar{\kappa}_{ii} = 0$ since $\bar{\kappa}_{ij}$ is antisymmetric. The noise operators can be expressed as a sum of contributions from the three reservoirs

$$c_{i,\text{in}}(t) = \sqrt{\frac{\kappa}{\kappa_i}} d_{\text{in}}^{(i)}(t) + \sum_{\alpha=1,2} \sqrt{\frac{\gamma_\alpha}{\kappa_i}} b_{\alpha,\text{in}}^{(i)}(t), \quad (\text{D4})$$

where the photon bath gives

$$\begin{aligned} d_{\text{in}}^{(i)}(t) &= \frac{1}{\sqrt{2\pi\rho_c}} \sum_j (V_{3,i} e^{-i\Delta_{c,j}(t-t_0)} g_{c,j} \\ &- V_{3,i+3} e^{i\Delta_{c,j}(t-t_0)} g_{c,j}^\dagger) \end{aligned} \quad (\text{D5})$$

and the mechanical baths give ($\alpha = 1, 2$)

$$b_{\alpha,\text{in}}^{(i)}(t) = \frac{V_{\alpha,i} + V_{\alpha,i+3}}{\sqrt{2\pi\rho_\alpha}} \sum_j e^{-i\omega_{\alpha,j}(t-t_0)} f_{\alpha,j}. \quad (\text{D6})$$

Here t_0 is the initial time (which can be taken in the distant past). The correlation functions of the noise operators

$$\langle c_{i,\text{in}}^\dagger(t) c_{i,\text{in}}(t') \rangle = n_i \delta(t - t') \quad (\text{D7})$$

are related to the occupation numbers n_i of the polariton modes. It is straightforward to compute Eq. (D7) from Eqs. (D4)–(D6). Using the reservoir thermal occupations $\langle f_{\alpha,i}^\dagger f_{\alpha,j} \rangle = \delta_{i,j} n_B(\omega_{\alpha,j})$ and $\langle g_{c,i}^\dagger g_{c,j} \rangle = 0$ (i.e., a zero-temperature optical bath), the expressions of n_i given in Eq. (14) are found.

In the regime which is most interesting for us, the energy differences $\omega_i - \omega_j$ between different polariton modes are at least of the same order as the mechanical frequencies. Taking $\kappa \ll \omega_{m1}, \omega_{m2}$, the effect of off-diagonal coupling induced by dissipation is suppressed by a small factor $\lesssim \kappa/\omega_{mi}$. This justifies considering the decoupled Heisenberg-Langevin equations (12) given in the main text. To show explicitly this argument, we consider the equation of motion for the off-diagonal Green's function $G_0^R[c_i, c_j^\dagger, t]$ (with $i \neq j$). From Eq. (D1) we get

$$\begin{aligned} \frac{d}{dt} G_0^R[c_i, c_j^\dagger, t] &= -\left(i\omega_i + \frac{\kappa_i}{2}\right) G_0^R[c_i, c_j^\dagger, t] \\ &- \sum_{i' \neq i} \left(\frac{\kappa_{ii'}}{2} G_0^R[c_{i'}, c_j^\dagger, t] + \frac{\bar{\kappa}_{ii'}}{2} G_0^R[c_{i'}^\dagger, c_j^\dagger, t] \right). \end{aligned} \quad (\text{D8})$$

To leading order, we can retain in the second line only the $i' = j$ term (i.e., neglect the off-diagonal and anomalous Green's functions). After a Fourier transform, we immediately find

$$G_0^R[c_i, c_j^\dagger, \omega] \simeq -\frac{i\kappa_{ij}/2}{(\omega - \omega_i + i\frac{\kappa_i}{2})(\omega - \omega_j + i\frac{\kappa_j}{2})}. \quad (\text{D9})$$

By evaluating the Green's function at the polariton frequency ω_i we find

$$\text{Im}G_0^R[c_i, c_j^\dagger, \omega_i] \simeq \kappa_i^{-1} \frac{\kappa_{ij}\kappa_j/2}{(\omega_i - \omega_j)^2}. \quad (\text{D10})$$

The diagonal Green's function gives $\text{Im}G_0^R[c_i, c_i^\dagger, \omega_i] = -2\kappa_i^{-1}$; thus Eq. (D10) is suppressed by a small factor approximately equal to $(\kappa/\omega_{mi})^2$. Nonlinear interactions will modify both $G_0^R[c_i, c_j^\dagger, \omega]$ and $G_0^R[c_i, c_i^\dagger, \omega]$ by introducing appropriate self-energies in the denominators. However, their relative strength will still be controlled by the same small factor.

APPENDIX E: ADIABATIC ELIMINATION OF THE CAVITY MODE

In the limit of large detuning, the cavity mode can be eliminated adiabatically to obtain an effective theory for the two mechanical modes. Here we refine Eq. (24), which is necessary to derive the effective dissipation rates and occupation numbers.

To perform the adiabatic elimination, we first consider the Heisenberg equation of the cavity mode $\dot{d} = i\Delta d - i\sum_i G_i(b_i + b_i^\dagger) - i\sum_i g_i d(b_i + b_i^\dagger)$. Since the adiabatic contribution to \dot{d} follows the slow mechanical motion, we approximate $\dot{d} = 0$ to get

$$d \simeq -\frac{\sum_i G_i(b_i + b_i^\dagger)}{|\Delta|} + \frac{g_1 [\sum_i G_i(b_i + b_i^\dagger)]^2}{G_1 \Delta^2}, \quad (\text{E1})$$

where we expanded the result to first order in g_i and used that $G_1/g_1 = G_2/g_2$. The first term recovers Eq. (24) and the second term is the leading correction in g_i . However, one can easily see that when substituting Eq. (E1) in the linear part of the Hamiltonian $H_0 \simeq -\Delta d^\dagger d + \sum_i G_i(d + d^\dagger)(b_i + b_i^\dagger) + \dots$ all the terms proportional to g_1 cancel each other. This is why, in practice, Eq. (24) gives the correct expression for g_{211} .

To treat the optical reservoir, however, Eq. (E1) is not sufficiently accurate. Instead of setting $\dot{d} = 0$, we perform a perturbative iteration and compute the leading contribution to \dot{d} from the first term of Eq. (E1). We obtain $\dot{d} \simeq -i\sum_i \omega_{mi} G_i(b_i - b_i^\dagger)/\Delta$, after using the equation of motion for the mechanical modes. Finally, substituting \dot{d} in the equation of motion of d , we obtain

$$d \simeq \frac{\sum_i G_i(b_i + b_i^\dagger)}{\Delta} - \frac{\sum_i \omega_{mi} G_i(b_i - b_i^\dagger)}{\Delta^2}. \quad (\text{E2})$$

Here we dropped the second term of Eq. (E1), which is justified when $\omega_{mi} \gg g_i$.

An alternative derivation relies on the Langevin equation for d , after setting $b_i = \tilde{b}_i e^{-i\omega_i t}$ and approximating the slowly varying operators \tilde{b}_i as constant. This yields

$$d \simeq \sum_i G_i \left(\frac{b_i}{\Delta + \omega_{mi} + i\frac{\kappa}{2}} + \frac{b_i^\dagger}{\Delta - \omega_{mi} + i\frac{\kappa}{2}} \right) + \tilde{d}_{\text{in}}, \quad (\text{E3})$$

where $\tilde{d}_{\text{in}} = -\sqrt{\kappa} \int_{-\infty}^t d\tau d_{\text{in}}(\tau) \exp[(i\Delta - \frac{\kappa}{2})(t - \tau)]$. In the limit $|\Delta| \gg \omega_{mi} \gg \kappa$ it is justified to neglect the effect of dissipation and expand Eq. (E3) in powers of ω_{mi}/Δ , thus recovering Eq. (E2).

Now we consider the coupling of the optical mode with the dissipative bath which, consistently with Appendix A, takes the form

$$H_{\text{diss},c} = -i \sqrt{\frac{\kappa}{2\pi\rho_c}} \sum_j [g_{c,j} d^\dagger - g_{c,j}^\dagger d]. \quad (\text{E4})$$

Using Eq. (E2), we obtain

$$\begin{aligned} H_{\text{diss},c} = & -i \sqrt{\frac{\kappa}{2\pi\rho_c}} \sum_{i=1,2} \frac{G_i}{\Delta} \\ & \times \sum_j \left[\left(1 - \frac{\omega_{mi}}{\Delta}\right) (g_{c,j} b_i^\dagger - g_{c,j}^\dagger b_i) \right. \\ & \left. + \left(1 + \frac{\omega_{mi}}{\Delta}\right) (g_{c,j} b_i - g_{c,j}^\dagger b_i^\dagger) \right], \quad (\text{E5}) \end{aligned}$$

which describes the desired interaction between mechanical modes and the reservoir of the cavity. For a zero-temperature reservoir, the cooling (heating) processes induced by the second (third) line of Eq. (E5) give the transition rates between Fock states

$$\Gamma_{n \rightarrow n-1}^{(i)} = \left[\gamma_i + \kappa \frac{G_i^2}{\Delta^2} \left(1 - \frac{\omega_{mi}}{\Delta}\right)^2 \right] n, \quad (\text{E6})$$

$$\Gamma_{n \rightarrow n+1}^{(i)} = \kappa \frac{G_i^2}{\Delta^2} \left(1 + \frac{\omega_{mi}}{\Delta}\right)^2 (n+1). \quad (\text{E7})$$

In Eq. (E6) we have included the effect of regular mechanical damping (at zero temperature). For an interaction of the type proportional to $g_{c,j}^\dagger b_i^\dagger$ heating by a zero-temperature reservoir would normally be impossible, due to conservation of energy (supposing $\Delta_{c,j} > 0$). However, we recall from the discussion leading to Eq. (A2) that the $g_{c,j}$ modes are defined in a frame rotating at the frequency ω_l of the driving laser and the frequency $\Delta_{c,j} > -\omega_l$ can be negative. This fact allows heating of the mechanical modes by excitation of a negative-frequency bath mode, which conserves the total energy (in the rotating frame). In physical terms, we see how this heating process is ultimately due to the presence of an optical drive, from which photons can be absorbed to excite the mechanical system.

Finally, we write the rates in Eqs. (E6) and (E7) in terms of energy dampings κ_i , which are given by Eq. (29), and average occupation numbers:

$$n_i = \left(1 - \frac{\omega_{mi}}{|\Delta|}\right)^2 \left(\frac{4\omega_{mi}}{|\Delta|} + \frac{|\Delta|^2 \gamma_i}{\kappa G_i^2}\right)^{-1}. \quad (\text{E8})$$

By neglecting $\omega_{mi}/|\Delta|$ in the first factor of Eq. (E8), we obtain Eq. (30). On the other hand, discarding the terms proportional to $\omega_{mi}/|\Delta|$ in the damping coefficients κ_i amounts to completely neglecting the optical bath, hence the importance of including the second correction in Eq. (E2). Equivalent results are obtained by inserting Eq. (E3) in the Langevin equations of the mechanical modes and extracting from there the effective parameters.

- [1] M. Aspelmeyer, T. J. Kippenberg, and F. Marquardt, Cavity optomechanics, *Rev. Mod. Phys.* **86**, 1391 (2014).
- [2] J. D. Teufel, T. Donner, D. Li, J. W. Harlow, M. S. Allman, K. Cicak, A. J. Sirois, J. D. Whittaker, K. W. Lehnert, and R. W. Simmonds, Sideband cooling of micromechanical motion to the quantum ground state, *Nature (London)* **475**, 359 (2011).
- [3] J. Chan, T. P. Mayer Alegre, A. H. Safavi-Naeini, J. T. Hill, A. Krause, S. Gröblacher, M. Aspelmeyer, and O. Painter, Laser cooling of a nanomechanical oscillator into its quantum ground state, *Nature (London)* **478**, 89 (2011).
- [4] J. B. Clark, F. Lecocq, R. W. Simmonds, J. Aumentado, and J. D. Teufel, Sideband cooling beyond the quantum backaction limit with squeezed light, *Nature (London)* **541**, 191 (2017).
- [5] A. H. Safavi-Naeini, S. Gröblacher, J. T. Hill, J. Chan, M. Aspelmeyer, and O. Painter, Squeezed light from a silicon micromechanical resonator, *Nature (London)* **500**, 185 (2013).
- [6] T. P. Purdy, P.-L. Yu, R. W. Peterson, N. S. Kampel, and C. A. Regal, Strong Optomechanical Squeezing of Light, *Phys. Rev. X* **3**, 031012 (2013).
- [7] E. E. Wollman, C. U. Lei, A. J. Weinstein, J. Suh, A. Kronwald, F. Marquardt, A. A. Clerk, and K. C. Schwab, Quantum squeezing of motion in a mechanical resonator, *Science* **349**, 952 (2015).
- [8] C. U. Lei, A. J. Weinstein, J. Suh, E. E. Wollman, A. Kronwald, F. Marquardt, A. A. Clerk, and K. C. Schwab, Quantum Non-demolition Measurement of a Quantum Squeezed State Beyond the 3 dB Limit, *Phys. Rev. Lett.* **117**, 100801 (2016).
- [9] R. W. Andrews, R. W. Peterson, T. P. Purdy, K. Cicak, R. W. Simmonds, C. A. Regal, and K. W. Lehnert, Bidirectional and efficient conversion between microwave and optical light, *Nat. Phys.* **10**, 321 (2014).
- [10] R. Riedinger, A. Wallucks, I. Marinković, C. Löschnauer, M. Aspelmeyer, S. Hong, and S. Gröblacher, Remote quantum entanglement between two micromechanical oscillators, *Nature (London)* **556**, 473 (2018).
- [11] C. F. Ockeloen-Korppi, E. Damskägg, J.-M. Pirkkalainen, M. Asjad, A. A. Clerk, F. Massel, M. J. Woolley, and M. A. Sillanpää, Stabilized entanglement of massive mechanical oscillators, *Nature (London)* **556**, 478 (2018).
- [12] S. Gröblacher, K. Hammerer, M. R. Vanner, and M. Aspelmeyer, Observation of strong coupling between a micromechanical resonator and an optical cavity field, *Nature (London)* **460**, 724 (2009).
- [13] J. D. Teufel, D. Li, M. S. Allman, K. Cicak, A. J. Sirois, J. D. Whittaker, and R. W. Simmonds, Circuit cavity electromechanics in the strong-coupling regime, *Nature (London)* **471**, 204 (2011).
- [14] E. Verhagen, S. Deléglise, S. Weis, A. Schliesser, and T. J. Kippenberg, Quantum-coherent coupling of a mechanical oscillator to an optical cavity mode, *Nature (London)* **482**, 63 (2012).
- [15] G. A. Peterson, S. Kotler, F. Lecocq, K. Cicak, X. Y. Jin, R. W. Simmonds, J. Aumentado, and J. D. Teufel, Ultrastrong Parametric Coupling Between a Superconducting Cavity and a Mechanical Resonator, *Phys. Rev. Lett.* **123**, 247701 (2019).
- [16] P. Rabl, Photon Blockade Effect in Optomechanical Systems, *Phys. Rev. Lett.* **107**, 063601 (2011).
- [17] A. Nunnenkamp, K. Børkje, and S. M. Girvin, Single-Photon Optomechanics, *Phys. Rev. Lett.* **107**, 063602 (2011).
- [18] A. Kronwald and F. Marquardt, Optomechanically Induced Transparency in the Nonlinear Quantum Regime, *Phys. Rev. Lett.* **111**, 133601 (2013).
- [19] Y.-C. Liu, Y.-F. Xiao, Y.-L. Chen, X.-C. Yu, and Q. Gong, Parametric Down-Conversion and Polariton Pair Generation in Optomechanical Systems, *Phys. Rev. Lett.* **111**, 083601 (2013).
- [20] X. Xu, M. Gullans, and J. M. Taylor, Quantum nonlinear optics near optomechanical instabilities, *Phys. Rev. A* **91**, 013818 (2015).
- [21] K. Børkje, A. Nunnenkamp, J. D. Teufel, and S. M. Girvin, Signatures of Nonlinear Cavity Optomechanics in the Weak Coupling Regime, *Phys. Rev. Lett.* **111**, 053603 (2013).
- [22] M.-A. Lemonde, N. Didier, and A. A. Clerk, Nonlinear Interaction Effects in a Strongly Driven Optomechanical Cavity, *Phys. Rev. Lett.* **111**, 053602 (2013).
- [23] M.-A. Lemonde and A. A. Clerk, Real photons from vacuum fluctuations in optomechanics: The role of polariton interactions, *Phys. Rev. A* **91**, 033836 (2015).
- [24] M.-A. Lemonde, N. Didier, and A. A. Clerk, Enhanced nonlinear interactions in quantum optomechanics via mechanical amplification, *Nat. Commun.* **7**, 11338 (2016).
- [25] L.-J. Jin, J. Qiu, S. Chesi, and Y.-D. Wang, Enhanced nonlinear interaction effects in a four-mode optomechanical ring, *Phys. Rev. A* **98**, 033836 (2018).
- [26] X.-Y. Lü, Y. Wu, J. R. Johansson, H. Jing, J. Zhang, and F. Nori, Squeezed Optomechanics with Phase-Matched Amplification and Dissipation, *Phys. Rev. Lett.* **114**, 093602 (2015).
- [27] T.-S. Yin, X.-Y. Lü, L.-L. Zheng, M. Wang, S. Li, and Y. Wu, Nonlinear effects in modulated quantum optomechanics, *Phys. Rev. A* **95**, 053861 (2017).
- [28] P. Kómár, S. D. Bennett, K. Stannigel, S. J. M. Habraken, P. Rabl, P. Zoller, and M. D. Lukin, Single-photon nonlinearities in two-mode optomechanics, *Phys. Rev. A* **87**, 013839 (2013).
- [29] M. Ludwig, A. H. Safavi-Naeini, O. Painter, and F. Marquardt, Enhanced Quantum Nonlinearities in a Two-Mode Optomechanical System, *Phys. Rev. Lett.* **109**, 063601 (2012).
- [30] A. Xuereb, C. Genes, and A. Dantan, Strong Coupling and Long-Range Collective Interactions in Optomechanical Arrays, *Phys. Rev. Lett.* **109**, 223601 (2012).
- [31] A. Xuereb, C. Genes, and A. Dantan, Collectively enhanced optomechanical coupling in periodic arrays of scatterers, *Phys. Rev. A* **88**, 053803 (2013).
- [32] J. Li, A. Xuereb, N. Malossi, and D. Vitali, Cavity mode frequencies and strong optomechanical coupling in two-membrane cavity optomechanics, *J. Opt.* **18**, 084001 (2016).
- [33] P. Piergentili, L. Catalini, M. Bawaj, S. Zippilli, N. Malossi, R. Natali, D. Vitali, and G. D. Giuseppe, Two-membrane cavity optomechanics, *New J. Phys.* **20**, 083024 (2018).
- [34] G. A. Peterson, F. Lecocq, K. Cicak, R. W. Simmonds, J. Aumentado, and J. D. Teufel, Demonstration of Efficient Nonreciprocity in a Microwave Optomechanical Circuit, *Phys. Rev. X* **7**, 031001 (2017).
- [35] N. R. Bernier, L. D. Toth, A. Koottandavida, M. A. Loannou, D. Malz, A. Nunnenkamp, A. K. Feofanov, and T. J. Kippenberg, Nonreciprocal reconfigurable microwave optomechanical circuit, *Nat. Commun.* **8**, 604 (2017).
- [36] W. P. Bowen and G. J. Milburn, *Quantum Optomechanics* (CRC, Boca Raton, 2015).

- [37] C. K. Law, Interaction between a moving mirror and radiation pressure: A Hamiltonian formulation, *Phys. Rev. A* **51**, 2537 (1995).
- [38] M. Ludwig, K. Hammerer, and F. Marquardt, Entanglement of mechanical oscillators coupled to a nonequilibrium environment, *Phys. Rev. A* **82**, 012333 (2010).
- [39] S. Gröblacher, A. Trubarov, N. Prigge, G. D. Cole, M. Aspelmeyer, and J. Eisert, Observation of non-Markovian micromechanical Brownian motion, *Nat. Commun.* **6**, 7606 (2015).
- [40] J. R. Johansson, P. D. Nation, and F. Nori, QuTiP: An open-source Python framework for the dynamics of open quantum systems, *Comput. Phys. Commun.* **183**, 1760 (2012).
- [41] S. Weis, R. Rivière, S. Deléglise, E. Gavartin, O. Arcizet, A. Schliesser, and T. J. Kippenberg, Optomechanically induced transparency, *Science* **330**, 1520 (2010).
- [42] A. H. Safavi-Naeini, T. P. Mayer Alegre, J. Chan, M. Eichenfield, M. Winger, Q. Lin, J. T. Hill, D. E. Chang, and O. Painter, Electromagnetically induced transparency and slow light with optomechanics, *Nature (London)* **472**, 69 (2011).
- [43] M. C. Kuzyk and H. Wang, Controlling multimode optomechanical interactions via interference, *Phys. Rev. A* **96**, 023860 (2017).